Eur. Phys. J. D **24**, 97–100 (2003)
DOI: 10.1140/epjd/e2003-00113-x

THE EUROPEAN PHYSICAL JOURNAL D

Matrix embedded cobalt-carbon nano-cluster magnets: behavior as room temperature single domain magnets

N. Nishi[a], K. Kosugi, K. Hino, and T. Yokoyama

Institute for Molecular Science, Nishigo-naka 38, Myodaiji, Okazaki 444-8585, Japan

Received 10 September 2002
Published online 3 July 2003

Abstract. A new type of Co-C nanoparticles is synthesized from CH_2Cl_2 solution of $Co_4(CO)_{12}$ by heating up to 210 °C in a closed vessel. Transmission electron microscope (TEM) and electron energy loss spectroscopy (EELS) observation show that the particles are embedded in amorphous carbon and their average size is 12 nm. The radial structure function obtained from the extended X-ray absorption fine structure (EXAFS) of the Co K-edge absorption of the Co-C nanoparticles provides a Co-C average distance of 2.08 Å and the Co-Co distances of 3.18 Å and 3.9 (±0.2) Å. The particles exhibit the magnetic hysteresis curve with a coercive force of 200 Oe at 20 K and 260 Oe at 300 K. The temperature dependence of the magnetic susceptibility measured under zero-field cooling and 10 Oe field cooling conditions exhibits the behavior characteristic of a set of single magnetic domain nanomagnets in an amorphous carbon matrix.

PACS. 36.40.-c Atomic and molecular clusters – 36.40.Cg Electronic and magnetic properties of clusters – 36.40.Mr Spectroscopy and geometrical structure of clusters – 75.50.Tt Fine-particle systems; nanocrystalline materials

1 Introduction

Development of air-stable single magnetic domain room temperature magnets is an important target of the recent nanotechnology in relation to developing the smallest information storage device and medical material transportation devices. Recent important progress in stabilizing cobalt nanomagnets has been made through carbon encapsulation of the metal particles [1–5]. The magnetic properties of these encapsulated metal nanoparticles exhibited the temperature change of the coercive force characteristic of metallic systems [3,4]. At lower temperatures the coercive force increased drastically. Single magnetic domain particles, however, are expected to show little temperature dependence of the coercive force, while the saturation magnetization of the single domain magnets increases. Single domain magnets in a matrix are also expected to interact with each other through magnetic dipole-dipole interaction minimizing the global magnetization of the system at zero magnetic firld. We report the preparation, characterization and magnetic properties of cobalt-carbon cluster nanomagnets working at room temperatures.

2 Experimental

A cobalt carbonyl compound, $Co_4(CO)_{12}$, is a good starting material for making Co-C clusters in solution. Cobalt atoms are expected to induce catalytic dissociation reactions of the solvent CH_2Cl_2 molecules at high temperatures. The carbonyl cluster compound is dissolved in CH_2Cl_2 and heated in dual tubes situated in a pressure resistant closed vessel up to 210 °C where the pressure reaches to 25 atm. After the quick cooling of the container by an electric wind fan, the solvent was transferred from the hot inner Pyrex tube to the outer Teflon tube. A Whatman narrow range indicator paper revealed that the pH of the transparent liquid was 1.0−1.5. Two kinds of solid products were seen in the inner tube: the layered solid attached on the tube wall at the levels lower than the original liquid surface, and the residual bulk solids on the bottom. A large part of the solids on the bottom was soluble in water. The pink crystals obtained by evaporating the solvent water were found to be cobalt dichloride, $CoCl_2$. The layered flaky solids on the wall were composed of carbonaceous cobalt compounds and cobalt dichloride. The IR spectrum taken as a KBr tablet showed the presence of unsaturated hydrocarbons and a large amount of water adsorbed in the solid. The flaky solids were washed by water very carefully and the black solids were dried in a vacuum container over two nights. The black fine powder with sizes of 1−5 μm was dispersed in an epoxy resin and sliced by 70 nm thick with a microtome, LEICA ULTRACUT UCT for scanning transmission electron microscope (STEM) and TEM observation by a JEOL JEM-2010F/STEM. Both sides of the sliced particles are free from the epoxy resin. The density of the magnetic particles in the matrix varies with changing the reaction conditions.

[a] e-mail: nishi@ims.ac.jp

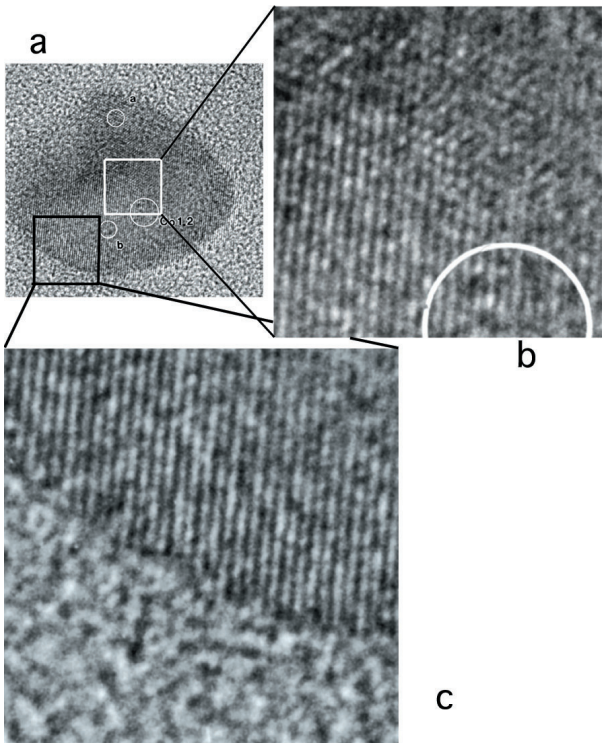

Fig. 1. A TEM image of a relatively large particle in the matrix. The upper part exhibits the disordered steps (image (b); see text). Image (c) shows the structural contrast of the nanoparticle to that of amorphous carbon. The scale of the expanded image (b) is 5 nm × 5 nm and that of the image (c) is 6 nm × 6 nm.

The magnetic material is very stable in the air at room temperature and the magnetic properties remains almost constant more than 6 months after the preparation.

3 Results and discussion

3.1 TEM and EELS observation

Figure 1 shows a TEM image of a relatively large nanocluster embedded in the matrix. Although most of the nanoparticles exhibited a single array of the lattice stripes (just like a single nanocrystal) as seen in the expanded image (c), the upper part of this particle shows disordered, thereby, three-dimensional "step" structure around the border region between the upper and the middle parts (expanded image (b)). The upper part was probably scraped off by the slicing knife of the microtome cutting machine. The image of the step area reminds us of a structure similar to NaCl type crystals. The expanded image (c) shows the interface region between the nanoparticle and the matrix. The matrix shows an amorphous structure, while the particle exhibits regular stripes of the lattice. The dark field TEM observation exhibited that the matrix is free from cobalt contamination as also seen in an electron energy loss spectrum (EELS) of the matrix area. Figure 2 shows the size distribution of the nanoparticles embedded

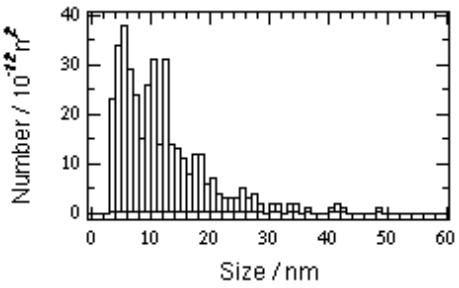

Fig. 2. Size distribution of the nanoparticles in the matrix. The size was obtained by assuming an elliptic shape for each particle area observed as the sum of the rectangular pixels.

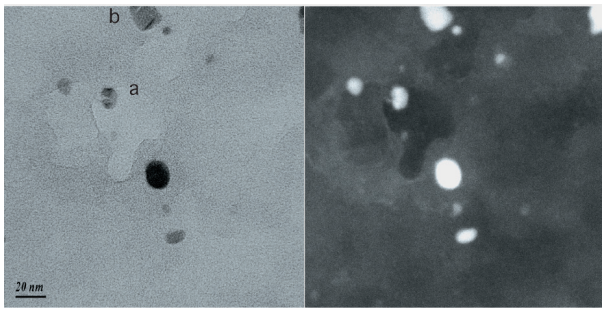

Fig. 3. Bright field STEM image (left) and HAADF image (right) of the Co-C nanoparticles embedded in the matrix.

in the matrix. The particle analysis was performed with a commercial softfare, IGOR Pro version 4.0. The particle size distribution provides us an average size of 11.8 nm. One can recognize, from the vertical scale of the distribution, how thin is the density of the nanoparticles in the matrix. In order to know the distribution of cobalt atoms, STEM images of the matrix-embedded particles are observed in high-angle annular dark field (HAADF) mode. In this mode, the widely scattered electron intensity is proportional to square of atomic numbers and the observed image is called "Z-contrast image". Figure 3 shows a comparison of a bright field image with the HAADF image. One can see the cobalt atoms concentrated in the particles. Figure 4 displays the electron energy loss spectra of the nanoparticle (a) and the matrix (b) observed with an electron beam size of 2.5 nm. The bottom frame shows that the Co-L bands at 781 and 796 eV are seen for the nanoparticle but the matrix does not show any signals of the Co component. The top frame covers the carbon K band and the oxygen K band regions. Any signal is not seen at the oxygen band region around 532−560 eV indicating that the clusters and the matrix are free from oxygen contamination even after the water treatment. The shape of the matrix C-K band is characteristic of amorphous carbon: the appearance of a weak peak due to π^* resonance at 285 eV and a broad band due to σ^* resonance at 297 eV [6]. The feature of the nanoparticle spectrum (solid line) at the C-K band region is very different from that of the matrix. The π^* resonance at 285 eV is much more enhanced and the peak position of the σ^* resonance shifted to 292 eV. This feature is very close to

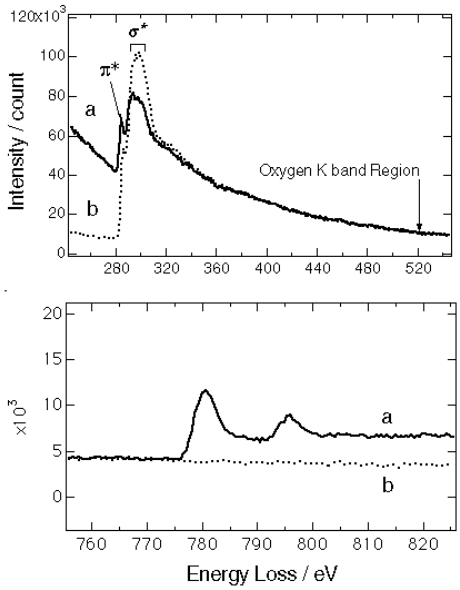

Fig. 4. Electron energy loss spectra of the nanoparticle (of which image is shown in Fig. 1, spectrum (a)) and the matrix (dotted spectrum (b)).

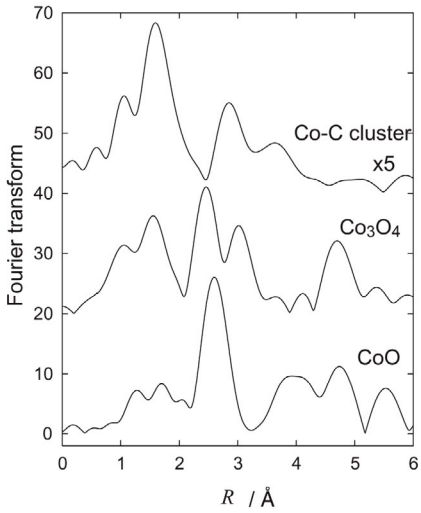

Fig. 5. Radial structure functions (RSF) obtained by Fourier transformation of EXAFS of the Co-C clusters in amorphous carbon, Co_3O_4 and CoO.

that of graphite and characteristic of unsaturated (*sp* or sp^2) carbon bonds [6]. On the basis of these EELS data in addition to the image feature seen in the TEM observation, we attribute the matrix to amorphous carbon and the nanoparticles to the Co-C clusters with carbon-carbon bonds.

3.2 EXAFS study

Figure 5 shows radial structure functions (RSF) obtained by Fourier transformation of extended X-ray absorption fine structure (EXAFS) appeared in the K-edge absorption spectra of the Co atoms of the Co-C clusters in amorphous carbon, Co_3O_4, and CoO. The latter two spectra of the oxides are displayed as references. Here, one can clearly see that the nanoparticles contain neither Co_3O_4 nor CoO. This is in consistent with the EELS observation. Since we know the correct Co-Co and Co-O distances for the two oxide compounds, we can obtain the phase shift factors for Co-Co distances. In the RSF's of Co_3O_4 and CoO, the strongest peaks correspond to the Co-Co distances of 2.87 Å and 2.99 Å, respectively. The two Co-Co peaks seen in the Co-C cluster function correspond to 3.18 Å and 3.9 (±0.2) Å. By assuming the same phase shift factor for the Co-C as that of Co-O, one can get the strongest Co-C peak of the Co-C clusters to be 2.08 Å. The RSF of the Co-C clusters shows the foot of the 2.08 Å peak at 2.514 Å that is the distance of the direct Co-Co bond in α and β form metallic cobalts [7,8]. The metallic radius for Co is reported to be 1.25 Å. Thus the peak at 2.08 Å cannot be attributed to any Co-Co bond [9]. It is quite reasonable that the acidic reaction condition cannot allow the existence of any metallic cobalt. The intensity of the Co-C peak is so strong suggesting that each Co atom can be surrounded with carbon atoms.

3.3 Reaction mechanism

In the present reaction, $CoCl_2$ and amorphous carbon are produced in addition to the Co-C cluster compound. The origin of the chloride and the carbon must be the solvent, CH_2Cl_2. Cobalt compounds show various catalytic activities including carbon-carbon coupling [10,11]. Cobaltocene is reported to dissociate CCl_4 producing cobaltocenium chloride, $(C_5H_5)_2Co^+$ Cl^- [10]. Long time heating or higher temperature reaction reduced the yields of the clusters resulting in the exclusion of the cobalt component from the carbonacious products. On the basis of these observation, we propose the following reaction sequence:
(1) cobalt-carbon cluster formation,

$$Co_4(CO)_{12} + 8CH_2Cl_2 \longrightarrow 4CoC_2 + 16HCl + 12CO\uparrow$$
$$4mCoC_2 \longrightarrow (CoC_2)_{4m}$$

(2) amorphous carbon production process.

$$(CoC_2)_{4n} + 8nHCl \longrightarrow 4nCoCl_2 + nC_8H_8.$$

It is well-known that the salt-like carbides of metals of the earlier periodic groups or the carbides of $4f$ and $5f$ elements form NaCl type crystal with $M^{2+}[C_2]^{2-}$ ionic components. CaC_2 is a typical example. In these carbides, $(C{\equiv}C)^{2-}$ behaves just like an atomic anion similar to CN^-. However, the chemical bonds in the Co-C_2 cluster are very different from that of CaC_2, because the d orbitals of Co must interact with π^* orbitals of the C_2 groups, forming d-π valence bonds.

3.4 Magnetic properties

Temperature changes of magnetic susceptibility (χ) of the matrix-embedded cobalt-carbon clusters are measured under the zero-field cooling (ZFC) condition and the field

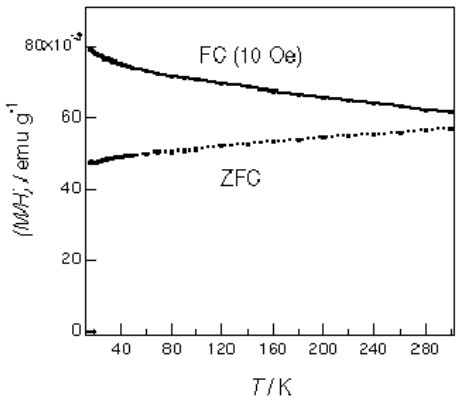

Fig. 6. Temperature change of magnetic susceptibility ($\chi = M/H$ (= 10 Oe)) of the matrix-embedded cobalt-carbon clusters measured under the zero-field cooling (ZFC) condition and the field cooling (FC) at 10 Oe.

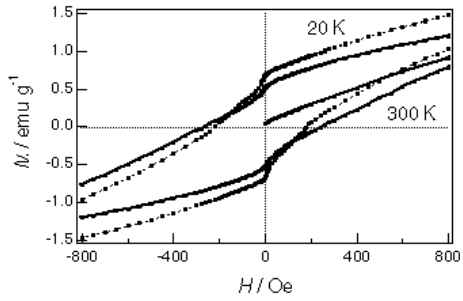

Fig. 7. Expanded view of magnetic hysteresis curves at 300 K and 20 K.

cooling (FC) at 10 Oe external magnetic field as shown in Figure 6. The susceptibility decreases with decreasing temperature at zero field, while under the field cooling condition it increases with decreasing temperature. This means that the 10 Oe external field aligns the magnetic moments of the particles along the field direction, although the magnetic moment of each particle is prone to align antiferromagnetically at zero field. The two curves (or lines) in Figure 6 behave just oppositely, and the average values are nearly temperature independent. The most important fact is seen in the hysteresis curves at 300 K and at 20 K as shown in Figure 7. The hysteresis changes continuously at the intermediate temperatures. Although the saturation magnetization and the residual magnetization become larger, the coercive force decreases at lower temperatures. The present system provides the coercive force to be 260 Oe at 300 K and 200 Oe at 20 K. This behavior is in marked contrast to that seen in the metallic system where the magnetic domain evolution is seen at lower temperatures. The size of the present particles in the former case is on the order of the single magnetic domain limit of $4 \sim 20$ nm [12,13]. The observed temperature dependence behaviors of the hysteresis and the susceptibility strongly suggest that the Co-C clusters are single magnetic domain magnets. The increase of the coercive force was seen when the reaction (2) was minimized by shortening the 210 °C heating time from 3 hours to 30 min. Then the coercive force of 510 Oe at 40 K and 370 Oe at 300 K were obtained. However the size distribution became more than two times wider, while the density became much denser.

3.5 Structure of Co-C_2 cluster

With the data available at this stage, we cannot determine the structure of the Co-C cluster conclusively. However, the high resolution TEM images, the EELS, the RSF, IR absorption and Raman scattering data can allow us to discuss the structure. Since the reaction condition is acidic at the high temperature producing Co^{2+} and Cl^- ions, the cobalt atoms in the cluster are thought to be in an oxidized (or cationic) state. We also observed the presence of π^* orbital(s) of the carbon atoms. At this stage, we present a linear chain model of -Co^{2+}-$C_2{}^{2-}$-Co^{2+}-$C_2{}^{2-}$-Co^{2+}– where each cobalt atom is surrounded with the C_2 groups of the four neighboring chains through strong d-π^* interaction with an octahedral configuration. This structure is similar to that of CaC_2. This cluster must be highly stabilized by charge transfer interactions and valence σ and d-π^* bond formation.

This work is supported by a program entitled "Research for the Future of Japan Society of the Promotion of Science" (RFTF: 99P01201).

References

1. E.M. Brunsman, R. Sutton, E. Bortz, S. Kirkpatrick, K. Midelfort, J. Williams, P. Smith, M.E. McHenry, S.A. Majetich, J.O. Artman, M. De Graef, S.W. Staley, J. Appl. Phys. **75**, 5882 (1994)
2. T. Hayashi, S. Hirono, M. Tomita, S. Umemura, Nature **381**, 772 (1996)
3. J.J. Host, J.A. Block, K. Parvin, V.P. Dravid, J.L. Alpers, T. Sezen, R. LaDuca, J. Appl. Phys. **83**, 793 (1998)
4. J.-M. Bonard, S. Seraphin, J.-E. Wegrowe, J. Jiao, A. Chatelain, Chem. Phys. Lett. **343**, 251 (2001)
5. J. Shi, M. Azumi, O. Nittono, Appl. Phys. A **73**, 215 (2001)
6. G. Comelli, J. Stohr, C.J. Robinson, W. Jark, Phys. Rev. B **38**, 7511 (1988)
7. D.R. Linde, *CRC Handbook of Chemistry and Physics*, 75th edn. (CRC press, 1995), Chap. 12
8. A.F. Wells, *Structural Inorganic Chemistry*, fifth edn. (Clarendon Press, Oxford, 1990), Chap. 29
9. A.F. Wells, *Structural Inorganic Chemistry*, fifth edn. (Clarendon Press, Oxford, 1990), Chap. 22
10. H.F. Klein, M. Mager, S. Isringhausen-Bley, U. Flörke, H.-J. Haupt, Organometallics **11**, 3174 (1992)
11. S. Katz, J.F. Weiher, A.F. Voigt, J. Am. Chem. Soc. **80**, 6459 (1958)
12. J. Frenkel, J. Dorfman, Nature **126**, 274 (1930)
13. A. Tonomura, T. Matsuda, J. Endo, T. Arii, K. Mihama, Phys. Rev. Lett. **44**, 1430 (1980)